Magma-shale interaction in large igneous provinces: implications for climate warming and sulfide genesis

Frances M. Deegan[1,2*], Jean H. Bédard[3], Stephen E. Grasby[4], Keith Dewing[4], Harri Geiger[1,5], Valeria Misiti[2], Manfredo Capriolo[6], Sara Callegaro[6], Henrik H. Svensen[6], Chris Yakymchuk[7], László E. Aradi[8], Carmela Freda[2,9], Valentin R. Troll[1,2]

[1]Department of Earth Sciences, Natural Resources and Sustainable Development (NRHU), Uppsala University, Uppsala, Sweden.
[2]Istituto Nazionale di Geofisica e Vulcanologia (INGV), Rome, Italy.
[3]Geological Survey of Canada (GSC), GSC-Québec, Québec, Canada.
[4]Geological Survey of Canada (GSC), GSC-Calgary, Calgary, Canada.
[5]Institute of Earth and Environmental Sciences, University of Freiburg, Freiburg im Breisgau, Germany.
[6]Centre for Earth Evolution and Dynamics, University of Oslo, Oslo, Norway.
[7]Department of Earth and Environmental Sciences, University of Waterloo, Waterloo, Canada.
[8]Lithosphere Fluid Research Laboratory, Faculty of Science, Eötvös Loránd University, Budapest, Hungary.
[9]European Plate Observing System (EPOS), European Research Infrastructure Consortium (ERIC), Rome, Italy.

*Corresponding author. Email: frances.deegan@geo.uu.se

Running title: Magma-shale interaction in LIPs

Manuscript for submission to *Journal of Petrology* as a *Letter*.

For potential inclusion in the Themed Article Collections *Large Igneous Provinces, Experimental Petrology*, and *Metamorphic Reactions and Metamorphic Fluids*.

ABSTRACT

Large Igneous Provinces (LIPs) whose magma plumbing systems intersect sedimentary basins are linked to upheavals of Earth's carbon and sulfur cycles and thus climate and life history. However, the underlying mechanistic links between these phenomena are elusive. We address this knowledge gap through short time-scale petrological experiments (1200 °C and 150 MPa) that explore interaction between basaltic melt and carbonaceous shale (mudstone) using starting materials from the Canadian High Arctic LIP and the Sverdrup Basin in which it intrudes. Here we show that entrainment of shale xenoliths in basaltic melt causes shale to shatter due to incipient thermal stress and devolatilization, which accelerates assimilation by increasing reactive surface area. Shale assimilation therefore facilitates transfer of sediment-derived volatile elements to the shallow parts of LIP plumbing systems, whereupon carbon dominates the vapor phase whilst sulfur is partitioned into sulfide melt droplets. This study reveals that although carbon and sulfur are efficiently mobilized as a consequence of shale assimilation, sulfides can sequester sulfur - an important climate cooling agent - thus enhancing net emissions of climate warming greenhouse gases by shale-intersecting LIPs.

Abstract word count: 180 words.

Keywords: *C cycle perturbations; High Arctic LIP (HALIP); large igneous provinces*; *magma-shale interaction*; *sulfide genesis*

Main text: 3555 words + figure captions: 462 words = total word count: 4017

INTRODUCTION

Large Igneous Provinces (LIPs) are comprised of massive emplacements of largely basaltic magma into Earth's lithosphere and onto the surface (Bryan and Ernst, 2008; Black *et al.*, 2021). Many LIP events coincide with environmental change and mass extinctions (Courtillot and Renne, 2003; Bond and Grasby, 2017; Ernst and Youbi, 2017), but the mechanisms underpinning this correlation are not fully understood (Bond and Grasby, 2017; Black *et al.*, 2021). The magnitude of carbon and sulfur released to the atmosphere is generally accepted as a key control on the severity of environmental impact of a LIP event (Jones *et al.*, 2015). However, there is active debate concerning whether the release of primary, mantle-derived volatiles by LIPs is sufficient to cause the global carbon cycle disruptions, climate change, and biotic crises that mark mass extinctions; or whether additional release of thermogenic, sediment-derived volatiles is required (Svensen *et al.*, 2004, 2007, 2009; Ganino and Arndt, 2009; Yallup *et al.*, 2013; Callegaro *et al.*, 2021; Capriolo *et al.*, 2021, 2022; Heimdal *et al.*, 2021).

It is therefore necessary to clarify the mechanisms, dynamics, and efficiency of volatile removal from sedimentary rocks that are intersected by LIP plumbing systems. However, study of magma-sediment interaction involving volatile-rich sedimentary rocks is fraught with obstacles such as poor outcrop preservation and accessibility. Sill-host rock contacts are often difficult to access and deeply weathered, sometimes necessitating collection of drill cores such as for the Siberian LIP (Callegaro *et al.*, 2021) and the Brazilian portion of Central Atlantic Magmatic Province (Heimdal *et al.*, 2019). Geochemical modelling of magma-sediment interaction is also limited, because whilst several platforms exist for modelling assimilation of silicate rocks, thermodynamic data for non-silicate materials, such as carbonates, coal, organic matter, and evaporitic sulfates and halides are lacking (Heinonen *et al.*, 2021). Efforts to study magma-sediment interaction through direct experimentation (using high pressure-temperature devices) has potential for generating unique mechanistic insights but has thus far largely been restricted to studies involving magmatic assimilation of carbonates (Freda *et al.*, 1997, 2008, 2010; Iacono Marziano *et al.*, 2007, 2008; Mollo *et al.*, 2010; Deegan *et al.*, 2010, 2016; Jolis *et al.*, 2013; Carter and Dasgupta, 2015, 2016, 2018), although there is growing interest in non-carbonate lithologies too (e.g. Iacono-Marziano *et al.*, 2017). Many of these previous studies utilized relatively long-duration experiments, with run times ranging from several hours to days, which yielded equilibrium melt-gas assemblages that can be difficult to interpret in terms of process.

Short-duration (seconds to minutes) petrological experiments that better replicate the onset of magma-sediment interaction emerged in the early 2010s (Deegan *et al.*, 2010) and paved the way

for close examination of the rapid transformations that occur when basaltic melt first comes into contact with sedimentary rock. In this paper, we apply a similar philosophy to simulate entrainment of carbonaceous mudstone (hereafter referred to as "shale") xenoliths in basaltic melt and explore incipient magma-shale interaction at LIPs. The experiments preserve textural and chemical information that is largely obliterated in longer duration experiments as well as in many natural contexts, which rarely freeze-in prograde reaction paths (**Fig. 1a**). Magma-shale interaction moreover involves a sulfur component, which extends its relevance to sulfide ore formation. It is generally accepted that sulfide formation in LIP-hosted Ni-Cu-PGE (Platinum Group Element) deposits often involved incorporation of sedimentary crustal sulfur during magma emplacement (Lesher, 2019). Since the solubility of sulfide in silicate melts is low, most of the sulfur needed to constitute Ni-Cu-PGE ore bodies calls for addition of crustal sulfur as sulfide "xenomelt(s)", i.e., a foreign melt derived from crustal rocks or xenoliths (Lesher, 2017, 2019). The crustal origin of sulfur is supported by isotopic and geochemical data but uncertainty remains surrounding how sulfide xenomelts form and are transported in ore-forming systems (Hayes *et al.*, 2015; Lesher, 2017, 2019). These are questions that short-duration high pressure-temperature interaction experiments can also potentially clarify.

FIELD AREA, STARTING MATERIALS, AND METHODS

Here we employ the Cretaceous High Arctic LIP (HALIP) as a case study because its mafic sill province, representing the frozen remains of the conduit system formerly supplying flood basalts to the surface, is spectacularly preserved and exposed in the Canadian Arctic (Jowitt *et al.*, 2014; Evenchick *et al.*, 2015; Deegan *et al.*, 2018; Bédard *et al.*, 2021a, 2021b). Much of the Canadian portion of the HALIP was emplaced at ca. 120 Ma into the Sverdrup Basin, a sedimentary depocenter filled with up to 13 km of siliciclastic, evaporitic, and carbonaceous strata of Carboniferous to Paleogene age (Embry and Beauchamp, 2019). HALIP sills that invaded Sverdrup Basin sedimentary rocks collectively influenced basin-scale thermal evolution and development of regional oil and gas resources (Jones *et al.*, 2007; Goodarzi *et al.*, 2019) and possibly also sulfide ore formation (Jowitt *et al.*, 2014; Saumur *et al.*, 2016). The Middle Triassic Murray Harbour Formation forms part of the Sverdrup Basin fill and is dominated by black shale and siltstone, with subordinate calcareous and phosphatic interbeds. This unit is rich in Type II kerogen and is considered to be the primary source rock for hydrocarbon discoveries in the Sverdrup Basin (Brooks *et al.*, 1992; Kondla *et al.*, 2015).

We utilized natural HALIP magmatic rock and Murray Harbour Formation shale as the experimental starting materials. The experimental conditions and compositions of the starting materials are provided in the **Supporting Data File**. Details of the experimental method and

analytical techniques applied to the experimental products are provided in full in the **Supporting Information**. To summarise, the magmatic starting material is a pristine, non-cumulate mafic rock sample from a ca. 30 m thick sill with 6.6 wt.% MgO and 0.15 wt.% S. The shale is a finely clastic mudstone collected from a site over 60 m perpendicular distance away from any observable sill contacts and contains 4.7 wt.% total organic carbon and 0.5 wt.% total S. The shale is principally composed of quartz (56 wt.%), calcite (24 wt.%), biotite (9 wt.%), dolomite (4 wt.%), and pyrite (1 wt.%) and has a loss on ignition (LOI) value of 21.6 wt.%, indicating that roughly one fifth of its mass comprises volatile compounds including sulfur from pyrite and organic matter at 0.5 wt.% plus inorganic and organic carbon.

The magmatic rock was converted to glass, both an anhydrous and a mildly hydrated aliquot, pulverized in an agate mill, and loaded into platinum capsules (ca. 25 to 35 mg of powdered glass per experiment) along with a solid fragment of shale (ca. 4 to 5 mg per experiment). Each capsule was positioned in a 19-25 mm NaCl-crushable MgO-borosilicate glass assembly employing a graphite furnace and was then pressurized to 150 MPa in a low-P calibrated non-end loaded piston cylinder (PC) device (see Masotta *et al.,* 2012). The assemblies were then heated to 1200 °C at a rate of 100 °C per minute and held at the set point temperature for durations of 0 s, 300 s, and 600 s while being continuously monitored for any P-T fluctuations. The experimental P-T conditions are considered appropriate for injection of HALIP tholeiites at or slightly above their liquidus (1100 to 1200 °C) at ca. 5 km depth in the Sverdrup Basin (see Bédard *et al.*, 2021a). The experiments were terminated by shutting down the power source whereafter they were isobarically quenched at a rate of ca. 100 °C per second in the first 5 seconds (to the glass transition) and ca. 33 °C per second thereafter. Fast, isobaric quenching is important to preserve textures and glass (≈melt) that formed in-situ within the time window of xenolith dissolution and melting (**Fig. 1a**). After quenching, the capsules were retrieved, cast in epoxy, polished, and inspected using SEM (Secondary Electron Microscopy). Quantitative analysis was subsequently performed utilising EPMA (Electron Probe Microanalysis) and Raman micro-spectroscopy for glass and volatile compositions, respectively (see **Supporting Information** for analytical details).

EXPERIMENTAL RESULTS

An extended description of the experimental products is provided in the **Supporting Information** and the compositions of the glasses and sulfides in the experimental products are provided in the **Supplementary Data File**. An overview of the textures of the experimental products is presented in **Fig. 1** as a series of SEM mosaic images and a summary of the compositions of the experimental

glasses, sulfides, and vapour bubbles are provided in **Figs. 2** and **3**. In brief, the experiments document features of incipient magma-shale interaction, including the following processes:

(i) Dissolution of shale into the host melt, manifest as disequilibrium textures and crustally contaminated, "modified" melts (**Figs. 1** and **2**).

(ii) Formation of modified melts that are initially restricted to patches within the shale fragment but eventually form a boundary layer surrounding shale. Calcium is enriched (relative to the starting HALIP basalt) in modified glass in all experiments whilst silica, potassium, and sulfur are often enriched too (**Fig. 2**).

(iii) Shattering and degassing of shale and formation of abundant vapor bubbles containing various carbon volatile species such as CO and CO_2 (**Fig. 3**).

(iv) Formation of sulfide mineralizations (≈ sulfide xenomelts) at magma-shale interfaces (**Figs. 2** and **3**).

The experiments therefore reveal that contaminated melts and carbon volatiles are generated rapidly as a consequence of shale assimilation but that sulfides effectively sequester sulfur, a climate cooling agent, thus enhancing net emissions of greenhouse gases by LIPs that intersect shale-bearing sedimentary basins (as discussed below).

DISCUSSION

Magma-sediment interaction in microcosm

Our experiments have replicated magma-shale interaction in microcosm, i.e., the experiments encapsulate in miniature the characteristics of a much larger system, as discussed here. Earlier, similarly designed experiments showed that magma-carbonate interaction results in a low viscosity, Ca-rich compositional boundary layer at the reaction site and a voluminous C-O-H (carbon-oxygen-hydrogen) vapor phase (e.g. Deegan *et al.*, 2010). We find evidence of this process in our experiments, but shale assimilation is complicated by the fact that shale contains silicate minerals and organic matter in addition to carbonate. Previous experimental work involving siliceous shale and/or clay showed that at low pressure, clay begins to melt at ca. 1200 °C, but disequilibrium melting of micas, quartz, and feldspar begins at ca. 700 to 800 °C, producing Si-rich partial melts (Wyllie and Tuttle, 1961; Nichols *et al.*, 1996; Erdmann *et al.*, 2007). Heating experiments have also recently shown that C-O-H-S fluids are generated from shale at temperatures ≤700 °C and that silicate melt is produced from ca. 800 °C (Virtanen *et al.*, 2021). None of these previous studies

simulated interaction between shale and basaltic melt, but there are nevertheless some broad similarities to our work. For instance, two of our experiments contain a separated high-silica glass phase (**Fig. 1b,c**), which we suggest is the product of quartz breakdown at <1200 °C during experiment heat-up. These segregated high-silica glass domains are not present in the mildly hydrated experiments, which suggests that melt mixing was more efficient at low temperatures (during heat-up) when there was water added to the basaltic melt.

Importantly, we observed a portion of Ca-enriched, compositionally modified (contaminated) glass near the reaction site in all of our magma-shale interaction experiments (**Fig. 2a,b**). The at times extremely high CaO content of this glass (45 wt.% max) indicates that the carbonate components of the shale dissolved rapidly into the host melt. In many experiments, the compositional boundary layers are also enriched in silica, potassium, and sulfur from dissolution of quartz, micas, and pyrite (**Fig. 2a,b**). These silica-rich contaminated melts are particularly significant because in natural systems they would likely crystallise zircon, which would enable U-Pb geochronology of basaltic magmas injected into shale (Gaynor *et al.*, 2022).

In addition to demonstrating local contamination phenomena, the experiments provide compelling evidence for transfer of carbon volatiles from shale to melt. Evidence of a vapor phase is preserved in the experiments as bubbles that coalesce and migrate within minutes. Our limited number of experiments do not allow us to quantify how vesicle volume changes as a function of reaction time, but the shale appears to undergo a significant volume change, with increasingly smaller fragments visible over time (**Fig. 1**). The volatile mix generated is comprised dominantly of C, CO, and CO_2 as revealed by spectroscopic analysis of small (ca. 20 µm diameter) subsurface bubbles in a zero-time experiment (**Fig. 3**). Methane and water may also be present, but further analyses would be required to verify this (cf. Capriolo *et al.*, 2021). Sulfur likewise cannot be ruled out as a vapour phase although it appears to be largely sequestered into sulfides that dot the melt-shale interface.

Thermal stresses and concentration of volatiles produced along cleavage planes in shale would trigger a localized volume change, which could lead to fragmentation of shale and open up new surface area for reaction, triggering a short-lived “run-away” effect with respect to volatile expulsion. Since the host melt is virtually incapable of storing dissolved CO_2 at 150 MPa (the solubility of CO_2 in basaltic magma at ca. 0.07 wt.%; Newman and Lowenstern, 2002), the system would quickly become fluid oversaturated and most of the carbon in the system would be expelled as a free vapor or fluid phase capable of hydrofracturing roof and wall rocks. Notably, thermodynamic models predict that assimilation of as little as 0.6 wt.% organic matter will cause a

doubling of the total volatile load of a magma and produce CO-dominated gases (Iacono-Marziano *et al.*, 2012). We have now verified these predictions via direct analysis of bubbles (**Fig. 3**) and provide unique empirical evidence for CO gas formation during magma-shale interaction.

Ground truthing the experimental results

There are several natural examples that mirror our experimental results, which we briefly summarise here: (i) Shale xenoliths reported from Nuussuaq (Greenland) and the Duluth Complex (USA) show evidence for extensive reaction and element exchange with their host melt (Pedersen and Larsen, 2006; Samalens *et al.*, 2017); (ii) Studies of mafic sills injected into shale in Skye (Scotland) show that shale close to sill contacts displays abundant vesicles, partial melt textures with glassy streaks enriched in sulfur, silica, and potassium, Fe-S mineralizations, and evidence for sulfur loss (Lindgren and Parnell, 2006; Yallup *et al.*, 2013); and (iii) Sill-shale contacts in the Canadian HALIP possess sulfides with textures similar to those reported here (see **Supporting Information**). These natural cases underscore both the utility of our experimental approach in understanding contact phenomena and the dynamic, rapidly evolving nature of magma-sediment interaction.

WIDER IMPLICATIONS

Formation of sulfide xenomelts

Thermodynamic models have shown that as little as 0.1 wt.% magmatic assimilation of organic matter (CH) will cause oxygen fugacity (fO_2) to decrease by more than two log-units (Iacono-Marziano *et al.*, 2012). Magmatic assimilation of shale therefore facilitates a reducing melt environment while also transferring sulfur from shale to the host melt. The calculated sulfur concentration at sulfide saturation (SCSS) is ca. 0.1 wt.% for the magmatic starting material at the P-T conditions of the experiments (Fortin *et al.*, 2015). These low solubilities indicate that the mafic host melt is ineffective as a carrier of sulfur at equilibrium conditions. Since only a minor amount of sulfur is soluble in the host melt, the excess sulfur would form a dense, immiscible sulfide "xenomelt" (Lesher, 2017, 2019). Some of the modified glasses in our experiments contain sulfur exceeding the SCSS (**Fig. 2a**), which is not surprising since the experiments clearly did not attain equilibrium. We therefore propose that crustally contaminated melts generated during incipient magma-shale interaction can temporarily carry excess sulfur, which may manifest as a fine suspension of sulfide droplets (i.e. sulfide xenomelts; **Fig. 2c** and **Fig. 4**). For the most part, the experiments are visualized here in two dimensions using SEM imaging of the surface. However, inspection of an experiment with extended focus under reflected light revealed a ca. 100 µm wide zone around shale replete with minute (<5 µm) sulfides beneath the sample surface (see **Supporting**

Information). This finding supports the notion that the compositional boundary layers in our experiments are a mixture of crustally contaminated silicate melt and fine disseminations of sulfide xenomelts. Our experiments therefore shed light on the origin of sulfide xenomelts in LIP systems that intersect sulfur-bearing sedimentary rocks. Moreover, the experiments support the idea that sulfur-charged contaminated melts can form rapidly, especially in fault-guided conduit systems where magmatic and tectonic brecciation would be common (Hayes *et al.*, 2015) and where they could be forced upward as a slug of sulfur-enriched magma. Since sulfide xenomelts can scavenge metals from mafic magmas, they may eventually lead to the formation of economic ore deposits.

Climate impact

Our experiments highlight that magma-shale interaction in the shallow plumbing systems beneath LIPs is an effective means to rapidly mobilize carbon volatiles (**Fig. 4**). Several major LIPs are characterized by pulsed emplacement of sills into sedimentary basins (e.g. Bédard *et al.*, 2021a, 2021b; Callegaro *et al.*, 2021), which would lead to repeated episodes of magma-sediment interaction and pulsed volatile release throughout the basin. These volatiles could then enter the sub-aerial or sub-aqueous environment via faults and/or hydrothermal vent complexes or breccia pipes, the latter of which are known from the Karoo (Svensen *et al.*, 2007) and Siberian LIP (Svensen *et al.*, 2018) and potentially the Barents Sea region of the HALIP too (Polteau *et al.*, 2016).

Climate warming induced by excess carbon outgassing at LIPs would cause thermal stress in ecosystems and potentially trigger ocean anoxic events (OAEs), a proximal killer in some mass extinction scenarios (Bond and Grasby, 2017). The HALIP was a protracted event spanning more than 40 myr with a major pulse of continental basaltic magmatism between 130-120 Ma and another at ca. 95 Ma (Bédard *et al.*, 2021a, 2021b). These pulses were coincident with OAE1a at 120 Ma and OAE2 at 95 Ma. OAE1a was accompanied by sea-surface warming of as much as 8 °C (Ando *et al.*, 2008), while OAE2 is considered to be one of the most intense OAEs (Naber *et al.*, 2020). Remarkably, the magnitude of sea-surface warming associated with OAE1a parallels that associated with the Paleocene-Eocene thermal maximum and the Jurassic Toarcian OAE, consistent with the idea that all of these environmental crises share a causal mechanism related to massive release of carbon to the atmosphere-ocean system (Ando *et al.*, 2008).

The driving force for OAE1a and OAE2 is suspected to be volcanic CO_2 outgassing (Méhay *et al.*, 2009; Midtkandal *et al.*, 2016; Naber *et al.*, 2020) but the source(s) remain uncertain. Possibilities include dissociation of methane clathrates or volcanism from the Ontong-Java LIP, the Caribbean LIP, or the HALIP (Méhay *et al.*, 2009; Midtkandal *et al.*, 2016; Naber *et al.*, 2020). The Barents Sea sill

complex, part of the wider HALIP, has been speculated as a source for potentially 20,000 Gt of thermogenic carbon (equivalent to 175 trillion oil barrels) via thermal metamorphism of up to 400,000 km^3 of organic-rich sediments due to repeated sill injection (Polteau *et al.*, 2016). This scenario assumes that a maximum of 2 wt.% of the carbon in thermal aureoles around sills was expelled (Polteau *et al.*, 2016), which would equate to ca. 4 wt.% original TOC assuming that no more than 50% original kerogen is converted to hydrocarbon. Employing a more conservative figure of 1 wt.% carbon discharged (= 2% original TOC), we arrive at 10,000 Gt thermogenic carbon released from the Barents Sea volcanic basin. Important to note is that these calculations do not consider inorganic carbon that could be effectively mobilized by heating of carbonates. Unfortunately, estimates of carbon release by HALIP intrusions are fraught with uncertainties regarding quantification of parameters such as thermal aureole thicknesses and stratigraphic variability in TOC. However, there are striking parallels between the estimated thermogenic carbon release for the Barents Sea (Polteau *et al.*, 2016) and for the Karoo LIP (Heimdal *et al.*, 2021).

In this study we employed on-land HALIP sills as a case study and provided experimental constraints that help clarify the mechanisms and rates of magma-shale interaction (summarised in **Fig. 4**). If we consider devolatilization of a cube of our starting material shale with 500 m side length, ca. 16 Mt of C could be produced. Given the short timescale of shale devolatilization observed here, and that magma volume of LIPs are on the order of 10^5 to 10^7 km^3 (Black *et al.*, 2021), it is wholly conceivable that several thousand Gt of C could be generated through repeated episodes of magma-shale interaction proximal to sills in a shallow magma plumbing system. This would moreover be in addition to decarbonation in the distal, lower-temperature parts of metamorphic aureoles (processes which are not directly addressed by our experiments). We therefore suggest that carbon release by magma-sediment interaction at various scales during emplacement of the Canadian Arctic portion of the HALIP could have been similar to estimates for thermogenic carbon release from the Barents Sea (up to 20,000 Gt C; Polteau *et al.*, 2016) or the Karoo (ca. 20,500 Gt C; Heimdal *et al.*, 2021), making the HALIP a strong contender as the causal mechanism for OAE1a and OAE2. However, detailed thermal modelling of the impact of widespread HALIP sill intrusion on Sverdrup Basin sediments would be required to test this hypothesis. A surprising corollary of our work is that entrapment of sulfur in sulfide xenomelts might act to lessen the amount of sulfur released to the atmosphere, which in turn, could boost the warming effects of carbon by producing fewer climate-cooling sulfurous aerosols. This may account for the general observation (cf. Bond and Grasby, 2017) of LIPs being more strongly associated with climate warming, rather than cooling.

ACKNOWLEDGEMENTS

We are grateful to the GEM-II (Geo-mapping for Energy and Minerals) program of the Geological Survey of Canada and to the Polar Continental Shelf Project for logistical support in the field. We also thank H. Behrens for synthesizing the hydrous starting material in Hannover (Germany), M. Nazzari for EPMA support at INGV Rome (Italy), M. Choquette for EPMA analyses at Université Laval (Canada), and C. Szabó for access to the Raman micro spectroscopy laboratory at Eötvös Loránd University of Budapest (Hungary). We are grateful to C.M. Lesher for pre-reviewing our manuscript, to J. Heinonen, D. Harlov, and M. Gavrilenko for helpful formal reviews, and to T. Waight and G. Zellmer for editorial handling. This project was supported by a Swedish Research Council grant (2018-04933) to FMD.

DATA AVAILABILITY

The data underlying this article are available in the article and in its online supplementary material (Supporting Information PDF file and Supporting Data File in Excel format).

REFERENCES *(reference count = 62)*

Ando, A., Kaiho, K., Kawahata, H. & Kakegawa, T. (2008). Timing and magnitude of early Aptian extreme warming: Unraveling primary δ18O variation in indurated pelagic carbonates at Deep Sea Drilling Project Site 463, central Pacific Ocean. *Palaeogeography, Palaeoclimatology, Palaeoecology* **260**, 463–476.

Bédard, J. H., Saumur, B. M., Tegner, C., Troll, V. R., Deegan, F. M., Evenchick, C. A., Grasby, S. E. & Dewing, K. (2021a). Geochemical systematics of High Arctic Large Igneous Province continental tholeiites from Canada - Evidence for progressive crustal contamination in the plumbing system. *Journal of Petrology* **62**, egab041.

Bédard, J. H., Troll, V. R., Deegan, F. M., Tegner, C., Saumur, B. M., Evenchick, C. A., Grasby, S. E. & Dewing, K. (2021b). High Arctic Large Igneous Province alkaline rocks in Canada: Evidence for multiple mantle components. *Journal of Petrology* **62**, egab042.

Black, B. A., Karlstrom, L. & Mather, T. A. (2021). The life cycle of large igneous provinces. *Nature Reviews Earth and Environment* **2**, 840–857.

Bond, D. P. G. & Grasby, S. E. (2017). On the causes of mass extinctions. *Palaeogeography, Palaeoclimatology, Palaeoecology* **478**, 3–29.

Brooks, P. W., Embry, A. F., Goodarzi, F. & Stewart, R. (1992). Organic geochemistry and biological marker geochemistry of Schei Point Group (Triassic) and recovered oils from the Sverdrup Basin

(Arctic Islands, Canada). *Bulletin of Canadian Petroleum Geology* **40**, 173–187.

Bryan, S. E. & Ernst, R. E. (2008). Revised definition of Large Igneous Provinces (LIPs). *Earth-Science Reviews* **86**, 175–202.

Callegaro, S. *et al.* (2021). Geochemistry of deep Tunguska Basin sills, Siberian Traps: correlations and potential implications for the end-Permian environmental crisis. *Contributions to Mineralogy and Petrology* **176**, 49.

Capriolo, M. *et al.* (2021). Massive methane fluxing from magma–sediment interaction in the end-Triassic Central Atlantic Magmatic Province. *Nature Communications* **12**, 5534.

Capriolo, M., Mills, B. J. W., Newton, R. J., Dal Corso, J., Dunhill, A. M., Wignall, P. B. & Marzoli, A. (2022). Anthropogenic-scale CO2 degassing from the Central Atlantic Magmatic Province as a driver of the end-Triassic mass extinction. *Global and Planetary Change* **209**, 103731.

Carter, L. B. & Dasgupta, R. (2015). Hydrous basalt-limestone interaction at crustal conditions: Implications for generation of ultracalcic melts and outflux of CO2 at volcanic arcs. *Earth and Planetary Science Letters* **427**, 202–214.

Carter, L. B. & Dasgupta, R. (2016). Effect of melt composition on crustal carbonate assimilation: Implications for the transition from calcite consumption to skarnification and associated CO2 degassing. *Geochemistry, Geophysics, Geosystems* **17**, 3893–3916.

Carter, L. B. & Dasgupta, R. (2018). Decarbonation in the Ca-Mg-Fe carbonate system at mid-crustal pressure as a function of temperature and assimilation with arc magmas – Implications for long-term climate. *Chemical Geology* **492**, 30–48.

Courtillot, V. E. & Renne, P. R. (2003). On the ages of flood basalt events. *Comptes Rendus - Geoscience* **335**, 113–140.

Deegan, F. M. *et al.* (2018). Impact of basaltic sills on sedimentary host rocks in the High Arctic Large Igneous Province. *European Geosciences Union*. Vienna, Austria EGU2018-17845.

Deegan, F. M., Troll, V. R., Freda, C., Misiti, V., Chadwick, J. P., McLeod, C. L. & Davidson, J. P. (2010). Magma-carbonate interaction processes and associated CO2 release at Merapi volcano, Indonesia: Insights from experimental petrology. *Journal of Petrology* **51**, 1027–1051.

Deegan, F. M., Troll, V. R., Whitehouse, M. J., Jolis, E. M. & Freda, C. (2016). Boron isotope

364 fractionation in magma via crustal carbonate dissolution. *Scientific Reports* **6**, srep30774.

365 Embry, A. & Beauchamp, B. (2019). *Sverdrup Basin*. *The Sedimentary Basins of the United States and*
366 *Canada*. Elsevier B.V.

367 Erdmann, S., London, D., Morgan VI, G. B. & Clarke, D. B. (2007). The contamination of granitic
368 magma by metasedimentary country-rock material: An experimental study. *Canadian*
369 *Mineralogist* **45**, 43–61.

370 Ernst, R. E. & Youbi, N. (2017). How Large Igneous Provinces affect global climate, sometimes cause
371 mass extinctions, and represent natural markers in the geological record. *Palaeogeography,*
372 *Palaeoclimatology, Palaeoecology* **478**, 30–52.

373 Evenchick, C. A., Davis, W. J., Bédard, J. H., Hayward, N. & Friedman, R. M. (2015). Evidence for
374 protracted High Arctic large igneous province magmatism in the central Sverdrup Basin from
375 stratigraphy, geochronology, and paleodepths of saucer-shaped sills. *Bulletin of the Geological*
376 *Society of America* **127**, 1366–1390.

377 Fortin, M. A., Riddle, J., Desjardins-Langlais, Y. & Baker, D. R. (2015). The effect of water on the sulfur
378 concentration at sulfide saturation (SCSS) in natural melts. *Geochimica et Cosmochimica Acta*
379 **160**, 100–116.

380 Freda, C., Gaeta, M., Giaccio, B., Marra, F., Palladino, D. M., Scarlato, P. & Sottili, G. (2010). CO2-
381 driven large mafic explosive eruptions: The Pozzolane Rosse case study from the Colli Albani
382 Volcanic District (Italy). *Bulletin of Volcanology* **73**, 241–256.

383 Freda, C., Gaeta, M., Misiti, V., Mollo, S., Dolfi, D. & Scarlato, P. (2008). Magma-carbonate
384 interaction: An experimental study on ultrapotassic rocks from Alban Hills (Central Italy). *Lithos*
385 **101**, 397–415.

386 Freda, C., Gaeta, M., Palladino, D. M. & Trigila, R. (1997). The Villa Senni Eruption (Alban Hills, central
387 Italy): The role of H2O and CO2 on the magma chamber evolution and on the eruptive scenario.
388 *Journal of Volcanology and Geothermal Research* **78**, 103–120.

389 Ganino, C. & Arndt, N. T. (2009). Climate changes caused by degassing of sediments during the
390 emplacement of Large Igneous Provinces. *Geology* **37**, 323–326.

391 Gaynor, S. P., Svensen, H. H., Polteau, S. & Schaltegger, U. (2022). Local melt contamination and
392 global climate impact: Dating the emplacement of Karoo LIP sills into organic-rich shale. *Earth*

393 *and Planetary Science Letters* **579**, 117371.

394 Goodarzi, F., Gentzis, T. & Dewing, K. (2019). Influence of igneous intrusions on the thermal maturity
395 of organic matter in the Sverdrup Basin, Arctic Canada. *International Journal of Coal Geology*
396 **213**, 103280.

397 Hayes, B., Bédard, J. H., Hryciuk, M., Wing, B., Nabelek, P., Macdonald, W. D. & Lissenberg, C. J.
398 (2015). Sulfide immiscibility induced by wall-rock assimilation in a fault-guided basaltic feeder
399 system, Franklin Large Igneous Province, Victoria Island (Arctic Canada). *Economic Geology* **110**,
400 1697–1717.

401 Heimdal, T. H., Callegaro, S., Svensen, H. H., Jones, M. T., Pereira, E. & Planke, S. (2019). Evidence for
402 magma–evaporite interactions during the emplacement of the Central Atlantic Magmatic
403 Province (CAMP) in Brazil. *Earth and Planetary Science Letters* **506**, 476–492.

404 Heimdal, T. H., Goddéris, Y., Jones, M. T. & Svensen, H. H. (2021). Assessing the importance of
405 thermogenic degassing from the Karoo Large Igneous Province (LIP) in driving Toarcian carbon
406 cycle perturbations. *Nature Communications* **12**, 6221.

407 Heinonen, J. S., Iles, K. A., Heinonen, A., Fred, R., Virtanen, V. J., Bohrson, A. & Spera, F. J. (2021).
408 From binary mixing to Magma Chamber Simulator - geochemical modeling of assimilation in
409 magmatic systems. In: Masotta, M., Beier, C. & Mollo, S. (eds) *Crustal Magmatic System*
410 *Evolution: Anatomy, Architecture and Physico-Chemical Processes*. American Geophysical
411 Union, 151–176.

412 Iacono-Marziano, G., Gaillard, F., Scaillet, B., Polozov, A. G., Marecal, V., Pirre, M. & Arndt, N. T.
413 (2012). Extremely reducing conditions reached during basaltic intrusion in organic matter-
414 bearing sediments. *Earth and Planetary Science Letters* **357**–**358**, 319–326.

415 Iacono Marziano, G., Gaillard, F. & Pichavant, M. (2007). Limestone assimilation and the origin of
416 CO2 emissions at the Alban Hills (Central Italy): Constraints from experimental petrology.
417 *Journal of Volcanology and Geothermal Research* **166**, 91–105.

418 Iacono Marziano, G., Gaillard, F. & Pichavant, M. (2008). Limestone assimilation by basaltic magmas:
419 An experimental re-assessment and application to Italian volcanoes. *Contributions to*
420 *Mineralogy and Petrology* **155**, 719–738.

421 Jolis, E. M., Freda, C., Troll, V. R., Deegan, F. M., Blythe, L. S., McLeod, C. L. & Davidson, J. P. (2013).

Experimental simulation of magma-carbonate interaction beneath Mt. Vesuvius, Italy. *Contributions to Mineralogy and Petrology* **166**, 1335–1353.

Jones, M. T., Jerram, D. A., Svensen, H. H. & Grove, C. (2015). The effects of large igneous provinces on the global carbon and sulphur cycles. *Palaeogeography, Palaeoclimatology, Palaeoecology* **441**, 4–21.

Jones, S. F., Wielens, H., Williamson, M. C. & Zentilli, M. (2007). Impact of magmatism on petroleum systems in the Sverdrup Basin, Canadian Arctic Islands, Nunavut: A numerical modelling study. *Journal of Petroleum Geology* **30**, 237–256.

Jowitt, S. M., Williamson, M. C. & Ernst, R. E. (2014). Geochemistry of the 130 to 80 Ma Canadian high arctic large igneous province (HALIP) event and implications for Ni-Cu-PGE prospectivity. *Economic Geology* **109**, 281–307.

Kondla, D., Sanei, H., Embry, A., Ardakani, O. H. & Clarkson, C. R. (2015). Depositional environment and hydrocarbon potential of the Middle Triassic strata of the Sverdrup Basin, Canada. *International Journal of Coal Geology* **147**–**148**, 71–84.

Lesher, C. M. (2017). Roles of xenomelts, xenoliths, xenocrysts, xenovolatiles, residues, and skarns in the genesis, transport, and localization of magmatic Fe-Ni-Cu-PGE sulfides and chromite. *Ore Geology Reviews* **90**, 465–484.

Lesher, C. M. (2019). Up, down, or sideways: emplacement of magmatic Fe–Ni–Cu–PGE sulfide melts in large igneous provinces. *Canadian Journal of Earth Sciences* **56**, 756–773.

Lindgren, P. & Parnell, J. (2006). Rapid heating of carbonaceous matter by igneous intrusions in carbon-rich shale, Isle of Skye, Scotland: An analogue for heating of carbon in impact craters? *International Journal of Astrobiology* **5**, 343–351.

Masotta, M., Freda, C., Paul, T. A., Moore, G. M., Gaeta, M., Scarlato, P. & Troll, V. R. (2012). Low pressure experiments in piston cylinder apparatus: Calibration of newly designed 25mm furnace assemblies to P=150MPa. *Chemical Geology* **312**–**313**, 74–79.

Méhay, S., Keller, C. E., Bermasconi, S. M., Weissert, H., Erba, E., Bottini, C. & Hochuli, P. A. (2009). A volcanic CO2 pulse triggered the Cretaceous oceanic Anoxic event 1a and a biocalcification crisis. *Geology* **37**, 819–822.

Midtkandal, I. *et al.* (2016). The Aptian (Early Cretaceous) oceanic anoxic event (OAE1a) in Svalbard,

Barents Sea, and the absolute age of the Barremian-Aptian boundary. *Palaeogeography, Palaeoclimatology, Palaeoecology* **463**, 126–135.

Mollo, S., Gaeta, M., Freda, C., Di Rocco, T., Misiti, V. & Scarlato, P. (2010). Carbonate assimilation in magmas: A reappraisal based on experimental petrology. *Lithos* **114**, 503–514.

Naber, T. V., Grasby, S. E., Cuthbertson, J. P., Rayner, N. & Tegner, C. (2020). New constraints on the age, geochemistry, and environmental impact of High Arctic Large Igneous Province magmatism: Tracing the extension of the Alpha Ridge onto Ellesmere Island, Canada. *Bulletin of the Geological Society of America* **133**, 1695–1711.

Newman, S. & Lowenstern, J. B. (2002). VolatileCalc: A silicate melt-H2O-CO2 solution model written in Visual Basic for excel. *Computers and Geosciences* **28**, 597–604.

Nichols, G. T., Wyllie, P. J. & Sternt, C. R. (1996). Experimental melting of pelagic sediment, constraints relevant to subduction. In: Bebout, G. E., Scholl, D. W., Kirby, S. H. & Platt, J. P. (eds) *Subduction: Top to bottom*. Americal Geophysical Union, 293–298.

Pedersen, A. K. & Larsen, L. M. (2006). The Ilugissoq graphite andesite volcano, Nuussuaq, central West Greenland. *Lithos* **92**, 1–19.

Polteau, S., Hendriks, B. W. H., Planke, S., Ganerød, M., Corfu, F., Faleide, J. I., Midtkandal, I., Svensen, H. S. & Myklebust, R. (2016). The Early Cretaceous Barents Sea Sill Complex: Distribution, 40Ar/39Ar geochronology, and implications for carbon gas formation. *Palaeogeography, Palaeoclimatology, Palaeoecology* **441**, 83–95.

Robertson, J., Ripley, E. M., Barnes, S. J. & Li, C. (2015). Sulfur liberation from country rocks and incorporation in mafic magmas. *Economic Geology* **110**, 1111–1123.

Samalens, N., Barnes, S. J. & Sawyer, E. W. (2017). The role of black shales as a source of sulfur and semimetals in magmatic nickel-copper deposits: Example from the Partridge River Intrusion, Duluth Complex, Minnesota, USA. *Ore Geology Reviews* **81**, 173–187.

Saumur, B. M., Dewing, K. & Williamson, M. C. (2016). Architecture of the Canadian portion of the high arctic large igneous province and implications for magmatic Ni–Cu potential. *Canadian Journal of Earth Sciences* **53**, 528–542.

Svensen, H. H., Frolov, S., Akhmanov, G. G., Polozov, A. G., Jerram, D. A., Shiganova, O. V., Melnikov, N. V., Iyer, K. & Planke, S. (2018). Sills and gas generation in the Siberian Traps. *Philosophical*

Transactions of the Royal Society A: Mathematical, Physical and Engineering Sciences **376**.

Svensen, H., Planke, S., Chevallier, L., Malthe-Sørenssen, A., Corfu, F. & Jamtveit, B. (2007). Hydrothermal venting of greenhouse gases triggering Early Jurassic global warming. *Earth and Planetary Science Letters* **256**, 554–566.

Svensen, H., Planke, S., Maithe-Sørensen, A., Jamtveit, B., Myklebust, R., Eidem, T. R. & Rey, S. S. (2004). Release of methane from a volcanic basin as a mechanism for initial Eocene global warming. *Nature* **429**, 542–545.

Svensen, H., Planke, S., Polozov, A. G., Schmidbauer, N., Corfu, F., Podladchikov, Y. Y. & Jamtveit, B. (2009). Siberian gas venting and the end-Permian environmental crisis. *Earth and Planetary Science Letters* **277**, 490–500.

Virtanen, V. J., Heinonen, J. S., Molnár, F., Schmidt, M. W., Marxer, F., Skyttä, P., Kueter, N. & Moslova, K. (2021). Fluids as primary carriers of sulphur and copper in magmatic assimilation. *Nature Communications* **12**, 6609.

Wyllie, P. J. & Tuttle, O. F. (1961). Hydrothermal Melting of Shales. *Geological Magazine* **98**, 56–66.

Yallup, C., Edmonds, M. & Turchyn, A. V. (2013). Sulfur degassing due to contact metamorphism during flood basalt eruptions. *Geochimica et Cosmochimica Acta* **120**, 263–279.

FIGURES AND CAPTIONS

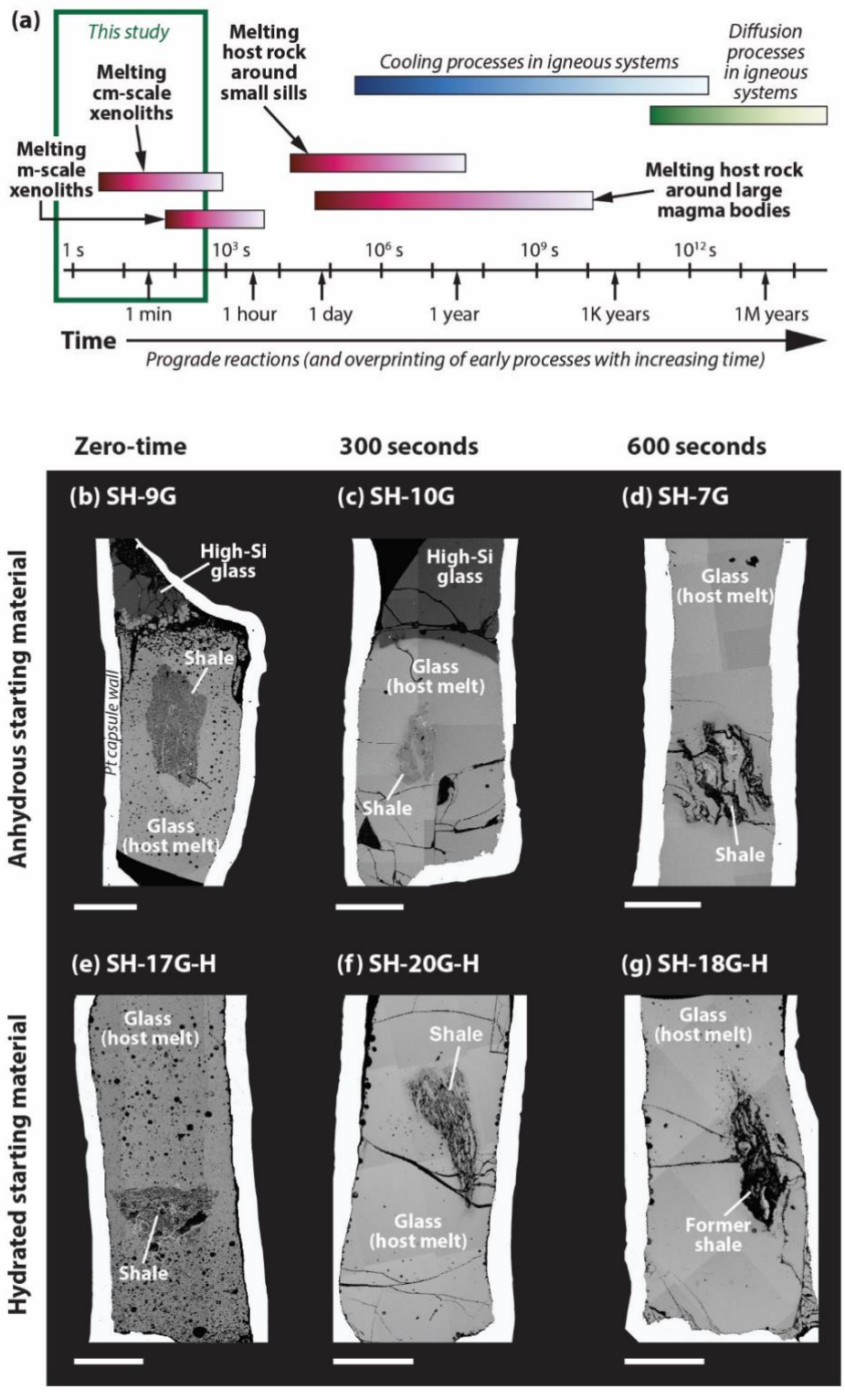

Figure 1. (a) Relative timescales for melting host rocks and xenoliths by magmatic intrusions (modified after Robertson *et al.*, 2015). This study targets the timeframe of cm- to m-scale xenolith melting in order to capture evidence of interaction processes that are only rarely preserved in nature. **(b)** to **(g)**

Backscattered electron (BSE) mosaic images of experimental run products. Intense degassing is evidenced by abundant small vesicles that permeate the run products (especially in the 0 s runs). Sulfides are generally found at magma-shale interfaces. Runs held for 600 s show a more advanced stage of shale dissolution into the host melt. Scale bars are 1 mm.

Figure 1 caption = 106 words.

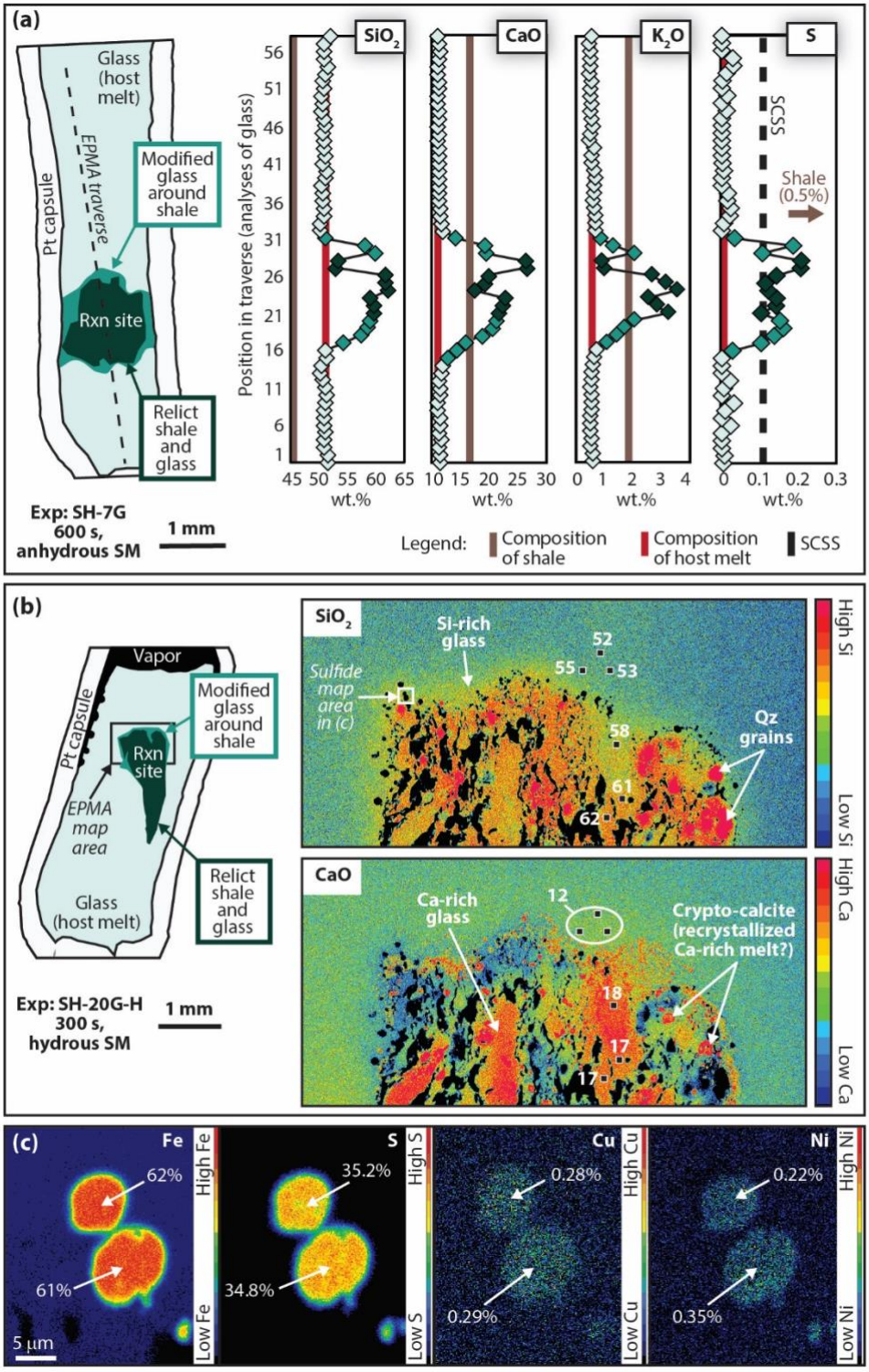

Figure 2. (a) Sketch of experiment SH-7G. To the right are EPMA glass data for SiO_2, CaO, K_2O, and S, respectively. **(b)** Sketch of experiment SH-20G-H. To the right are EPMA SiO_2 and CaO maps. Small black squares on the maps represent EPMA glass analysis sites and numeric values are in weight %. **(c)** EPMA Fe, S, Cu, and Ni maps for sulfides at the melt-shale interface (white box on SiO_2 map). Numeric values are in weight %. Abbreviations: Qz, quartz; Rxn, reaction; SCSS, sulfur concentration

518 at sulfide saturation; S.M., starting material. All EPMA glass data are normalized to 100% and the
519 glass and sulfide data are reported in **the Supplementary Data File**.
520
521 *Figure 2 caption = 113 words.*
522

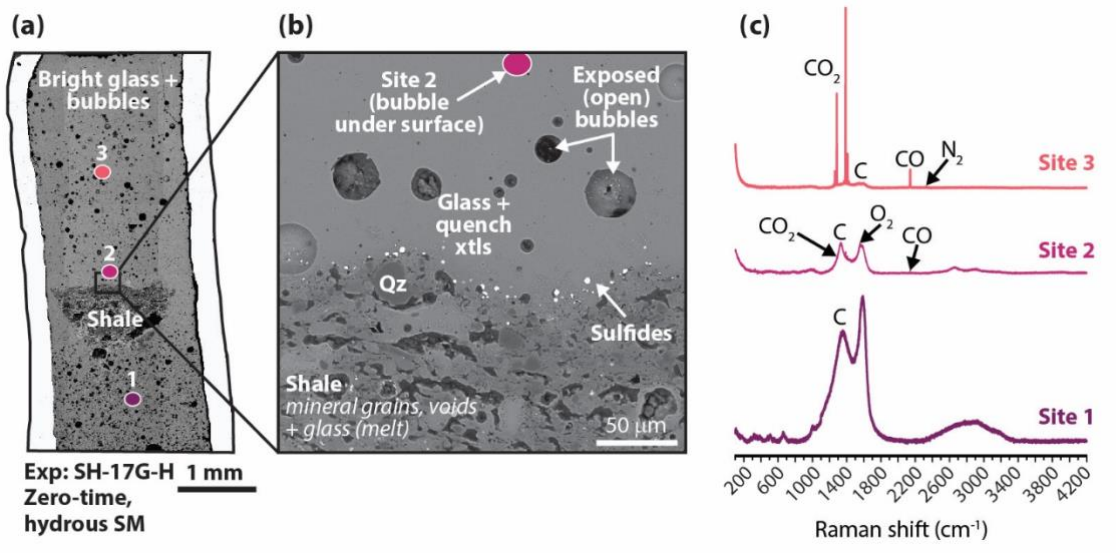

Figure 3. (a) BSE mosaic image of experiment SH-17G-H showing the locations of Raman analysis sites. **(b)** BSE image of the shale-melt interface showing the texture of partly dissolved shale, sulfides along the shale-melt boundary, and abundant bubbles in the glass. Note that this is a surface image and therefore the bubbles that are visible were opened during sample polishing. Raman analyses were conducted on in-tact bubbles beneath the sample surface. **(c)** Raman spectra for the analysis sites are shown to the right, with C, CO, CO_2, O_2, and N_2 bands identified (see **Supplementary Information** for further details).

Figure 3 caption = 98 words.

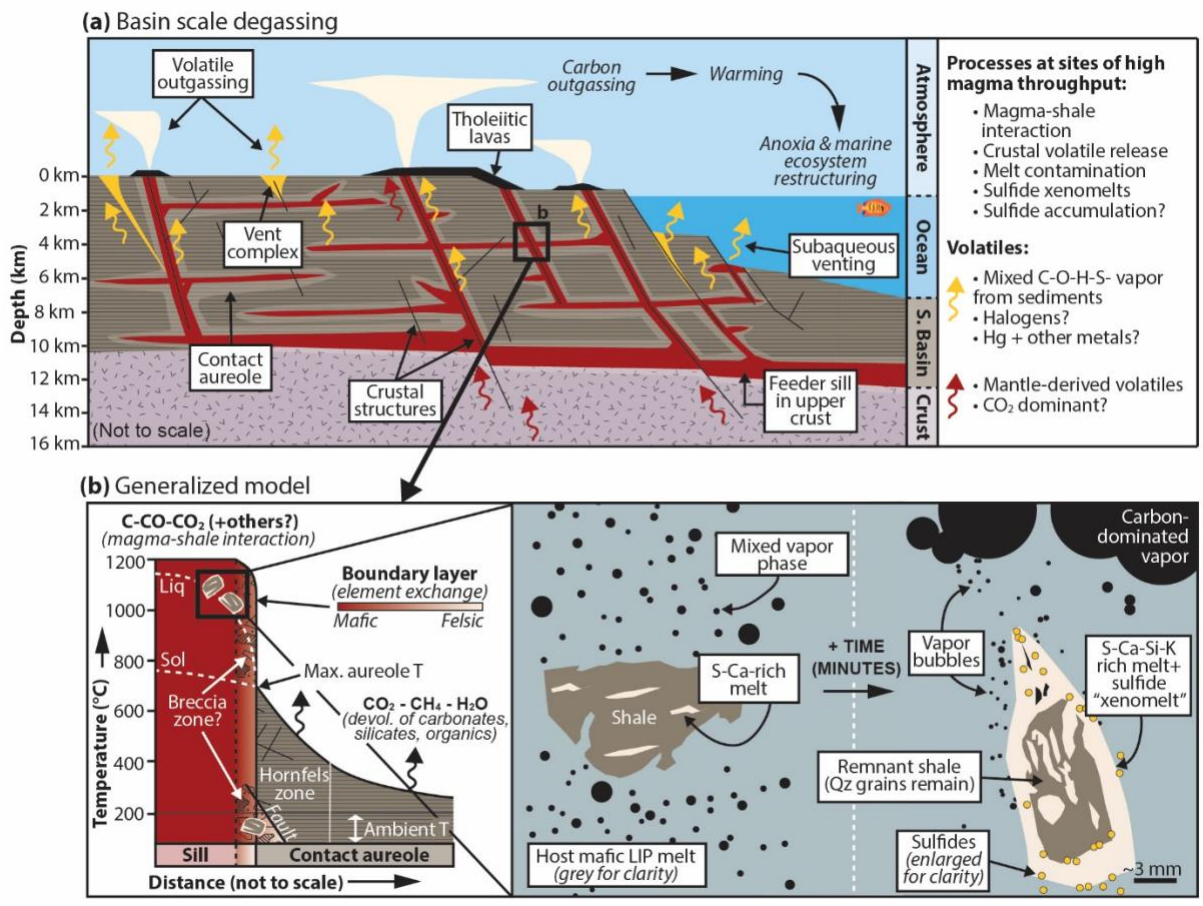

Figure 4. (a) Illustration of a LIP plumbing system intersecting a sedimentary basin. Sill injection into shale generates sediment-derived volatiles (fluids and/or vapour). If these volatiles enter the atmosphere and/or ocean through a vent complex or eruption, they can trigger climate warming and ocean anoxia. **(b)** Generalized model of sill-host rock interaction with a close-up of incipient magma-shale interaction as revealed by experiments. Magma-shale interaction causes formation of carbon volatiles, crustally contaminated melts, and sulfide xenomelts. Note that contact aureoles reach a maximum temperature (max. aureole T) of ~650°C depending on multiple factors including sill temperature, ambient temperature, sill thickness, and host rock type and are a source of volatiles not directly studied in our experiments. Sill liquidus and solidus curves are estimated based on HALIP petrological models (Bédard *et al.*, 2021a). Abbreviations: devol, devolatilization; Liq., liquidus; Sol, solidus; S. Basin, sedimentary basin; T, temperature.

Figure 4 caption = 145 words.